

# Electrical and structural properties of zinc substituted nickel ferrites synthesized by sol-gel technique

Sunita Khangembam, Maisnam Victory, Waikhom Surchandra, Sumitra Phanjoubam\*

*Department of Physics, Manipur University, Manipur, Canchipur, 795003, India*

\*Corresponding author, E-mail: sumitraphanjoubam@gmail.com; Tel: (+91) 9436894642

Received: 31 March 2016, Revised: 26 September 2016 and Accepted: 20 December 2016

DOI: 10.5185/amp.2017/306

www.vbripress.com/amp

## Abstract

Recent technological breakthroughs and the desire for new functions generate an enormous demand for synthesizing new materials through different ways and methods which show superior properties compared with their pure counterparts. Presently, polycrystalline zinc doped nickel ferrites having the compositional formula  $Ni_{1-x}Zn_xFe_2O_4$  where  $x = 0.0, 0.1, 0.2$  and  $0.4$  were synthesized. Sol-gel auto combustion method was adopted for the preparation of these ferrites since it provides a simple and economic alternative technique ensuring good stoichiometric control, production of particles with narrow size distribution in a relatively shorter time, good homogeneity and high sinterability at lower temperature. Structural studies were carried out by XRD. Various structural properties like lattice parameter, crystallite size and density were calculated from the XRD data. Micro structural studies were carried out using Scanning Electron Microscopy (SEM), while the elemental compositions of all the samples were studied by Energy Dispersive X-ray Analysis (EDAX). The frequency variation of room temperature dielectric constant and dielectric loss was studied in the frequency range 100Hz – 1MHz and dispersive behavior was observed. The room temperature dc resistivity of all the samples was also investigated. Zn substituted nickel ferrites are found to be useful in microwave and electronic devices. Copyright © 2017 VBRI Press.

**Keywords:** Ni ferrite, sol-gel, XRD, SEM, dielectric.

## Introduction

Ferrites with spinel structure are technologically important class of magnetic materials with  $Fe_2O_3$  as their main component having the general formula  $MFe_2O_4$  where M represents metallic cation like  $Zn^{2+}$ ,  $Co^{2+}$ ,  $Mg^{2+}$ ,  $Mn^{2+}$  etc. This class of materials bridges scientific discipline and combines the best attribute of the different world in one system. Recent investigations show many interesting properties of ferrites which are largely dependent upon the synthesis technique, nature of dopant, dopant concentration and heating conditions. Its property of versatility gives rise to a number of different types of ferrites with varied properties. Nickel ferrites have inverse spinel structure i.e. oxygen ions have cubic closed packing arrangement where Ni exhibits a strong octahedral site preference. Nickel and substituted nickel ferrites play significant role in technological applications such as microwave devices, power transformer in electronics, rod antenna, read/write heads for high speed digital tapes etc because of their high resistivity, low dielectric loss and high Curie temperature etc [1-5].

Among the various substituted nickel ferrites, NiZn ferrites are one of the most versatile soft magnetic materials. NiZn ferrite is a mixed spinel ferrite in which A –sites (tetrahedral sites) are occupied by

$Zn^{2+}$  and  $Fe^{3+}$ , B – sites (octahedral sites) are occupied by  $Ni^{2+}$  and  $Fe^{3+}$  ions. The compositional variation in these ferrites results in the redistribution of metal ions over the tetrahedral and octahedral sites which can modify their properties. Besides substitution, synthesis methods also greatly influence the properties of these ferrites [6-9]. Employment of chemical methods like sol-gel, co-precipitation, spray drying, citrate precursor, and hydrothermal methods other than the conventional ceramic method provides a simple and economic alternative, high degree of compositional homogeneity content in relatively short processing time at a very low temperature for preparation of ferrites with enhanced properties [10-13]. This paper focuses on the preparation of Zn substituted Ni ferrites by sol-gel technique with an aim to investigate the effect of substitution level on the structural, micro structural and electrical properties of the samples.

## Experimental

### Materials

The starting materials for the synthesis of zinc doped nickel ferrites include hexyhydrated zinc nitrate ( $Zn(NO_3)_2 \cdot 6H_2O$ , purity~96%) from Merck, Mumbai, hexyhydrated nickel nitrate ( $Ni(NO_3)_2 \cdot 6H_2O$ ,

purity~97%) from Merck, Mumbai, nanohydrated iron nitrate ( $\text{Fe}(\text{NO}_3)_2 \cdot 9\text{H}_2\text{O}$ , purity~98%) from Merck, Mumbai. The polyvinyl alcohol 1 (PVA) polymer powder from LOBA Chemie, Mumbai, the ethanediol (ethylene glycol) ( $\text{CH}_2(\text{OH})_2$ , purity~99%) from S.d. fine CHEM PVT.LTD., BOISAR and all the chemicals are used without further purification. The deionised (DI) water is used as solvent.

### Materials synthesis

For the preparation of polycrystalline nickel ferrites having compositional formula  $\text{Ni}_{1-x}\text{Zn}_x\text{Fe}_2\text{O}_4$  where  $x = 0.0, 0.1, 0.2$  and  $0.4$  employing sol-gel auto combustion technique stoichiometric ratios of Ni ( $\text{NO}_3)_2 \cdot 6\text{H}_2\text{O}$ , Zn ( $\text{NO}_3)_2 \cdot 6\text{H}_2\text{O}$  and Fe ( $\text{NO}_3)_3 \cdot 9\text{H}_2\text{O}$  are taken and dissolved in ethylene glycol in the ratio 3:1 to obtain the precursor solutions. The obtained precursor solution is then heated at  $40^\circ\text{C}$  with constant stirring until a clear solution is obtained. The temperature is increased to  $60^\circ\text{C}$  and finally to  $100^\circ\text{C}$ , till the solution starts to burn with the release of a lot of heat producing a highly voluminous fluffy product. The product so obtained is the as prepared nickel zinc ferrite powder. The obtained powder samples are pre-sintered at  $700^\circ\text{C}$  for 3 hours. This powder is then grounded and mixed with 3 wt. % of PVA which acts as a binder and then pressed into pellets with  $100\text{kg}/\text{cm}^3$  pressure for 5 mins. These pellets are finally sintered at  $1000^\circ\text{C}$  for 5 hours which are then used for various structural and electrical measurements.

### Characterizations

The single phase formation of the samples was confirmed by X-ray diffraction studies using a Philips X'pert Pro Pan Analytic XRD using  $\text{CuK}\alpha$  radiation of wavelength  $\lambda = 1.5406\text{\AA}$ , by varying angle ( $2\theta$ ) from  $20^\circ$  to  $80^\circ$ . The lattice parameter ( $a$ ) was calculated from the XRD data using the formula,

$$d = a / (h^2 + k^2 + l^2)^{1/2} \quad (1)$$

where, 'd' is the interplanar spacing and (h k l) the miller indices. The crystallite size (D) was determined from the XRD data using the Debye-Scherrer's formula,

$$D = 0.94 \lambda / \beta \cos \theta \quad (2)$$

where,  $\lambda$  is the wavelength of Cu target ( $\lambda=15.406\text{nm}$ ),  $\beta$  the full width at half maximum and  $\theta$  the Bragg's diffraction angle. The X-ray density ( $d_x$ ) was calculated using the formula,

$$d_x = 8M / Na^3 \quad (3)$$

where, 'M' is the molecular mass and 'N' the Avogadro's number. The microstructure of the

samples was recorded using Scanning Electron Microscope (SEM FEI QUANTA-250), while the elemental compositions of all the samples were studied by Energy Dispersive X-ray Analysis (EDAX). Electrical contacts were made on both sides of the flat surfaces of each pellet using silver coatings for ohmic contact. Dielectric measurements were done on these pellets using Agilent HP 4284 A LCR meter as a function of frequency in the range 100Hz to 1MHz. The corresponding loss tangent,  $\tan\delta$ , was also simultaneously recorded. The room temperature resistance of each composition was measured using a multimeter. From the observed value of R, the room temperature dc resistivity ( $\rho$ ) was evaluated using the formulas.  $\rho = RA/d$  where A is the area and d the thickness of the sample.

## Results and discussion

### X-ray diffraction analysis

The typical XRD pattern for  $\text{Ni}_{1-x}\text{Zn}_x\text{Fe}_2\text{O}_4$  samples for  $x = 0.0, 0.1, 0.2$  and  $0.4$  are depicted in **Fig. 1** showing main intensity peaks corresponding to specific planes (220), (311), (400), (422), (511) and (440) without any extra lines which confirms the single phase spinel structure of all the samples planes.

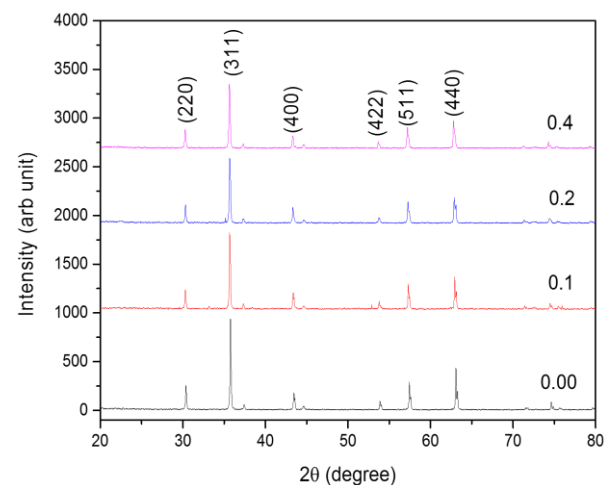


**Fig.1.** XRD pattern for  $\text{Ni}_{1-x}\text{Zn}_x\text{Fe}_2\text{O}_4$  ferrites for  $x =$  a) 0.0, b) 0.1 c) 0.2 and d) 0.4.

Various structural properties like lattice parameter and crystallite size are calculated from the XRD data and are listed in **Table 1**.

**Table 1.** Structural data for  $\text{Ni}_{1-x}\text{Zn}_x\text{Fe}_2\text{O}_4$  ferrites sintered at  $1000^\circ\text{C}$ .

Composition (x)	Lattice parameter 'a' (Å)	Crystallite size 'D' (nm)	Theoretical density 'd <sub>x</sub> ' (g/cm <sup>3</sup> )
0.0	8.325	171.90	5.40
0.1	8.344	163.43	5.34
0.2	8.347	128.39	5.38
0.4	8.354	143.69	5.36

It is observed that the lattice parameter increases with the increase of  $Zn^{2+}$  content. This can be attributed to the fact that  $Ni^{2+}$  ions with ionic radii 0.78Å have been replaced by  $Zn^{2+}$  ions of larger ionic radius 0.82Å. Since larger ions are replacing the smaller ones, an increase in the lattice parameter is expected [14]. The crystallite size was found to decrease with the increase of  $Zn^{2+}$  content.

### SEM and EDAX analysis

**Fig. 2** shows the SEM photomicrographs for  $Ni_{1-x}Zn_xFe_2O_4$  samples for  $x = 0.0, 0.1, 0.2$  and  $0.4$ , depicting well defined grains. The average grain size of the samples was found to be in the range 350-500 nm. These samples prepared by the chemical method showed grain size which is much reduced from that of ferrites prepared by conventional ceramic method (~ order of micrometer) [15].

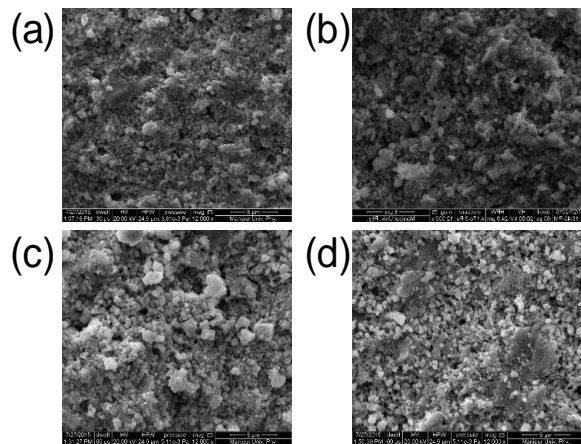


**Fig. 2.** SEM photomicrographs for  $Ni_{1-x}Zn_xFe_2O_4$  ferrites for  $x =$  (a) 0.0, (b) 0.1 (c) 0.2 and (d) 0.4.

The study of energy dispersive analysis of X-ray of the samples confirms the chemical composition and stoichiometric proportions. The typical EDAX spectra for  $x=0.2$  is shown in **Fig. 3** and the compositional percentage of  $Zn^{2+}$ ,  $Ni^{2+}$ ,  $Fe^{3+}$  and  $O^{2-}$  is listed in **Table 2**. Existence of impurity phase has not been observed. The ions present in  $Ni_{1-x}Zn_xFe_2O_4$  where  $x = 0.0, 0.1, 0.2$  and  $0.4$  are observed to be in stoichiometric proportions.

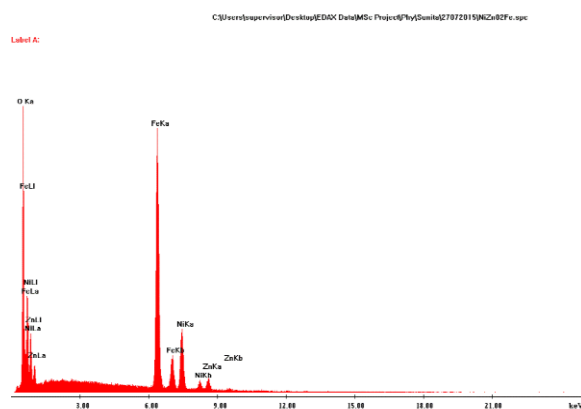


**Fig. 3.** EDAX spectra of  $Ni_{1-x}Zn_xFe_2O_4$  ferrites ( $x=0.2$ )

**Table 2.** Elemental percentage in  $Ni_{1-x}Zn_xFe_2O_4$  ferrites.

Composition	$Ni^{2+}$ (%)	$Zn^{2+}$ (%)	$Fe^{3+}$ (%)	$O^{2-}$ (%)
0.0	12.73	0.00	28.89	58.38
0.1	10.97	1.28	27.74	60.00
0.2	10.76	2.68	29.92	56.65
0.4	9.76	4.33	32.51	53.39

### Dielectric properties study

The dependence of dielectric constant of Ni-Zn ferrites as a function of frequency in the range 100Hz- 1M Hz as observed in **Fig. 4** shows a dispersive behavior. This behavior can be explained in terms of Maxwell-Wagner type of interfacial polarization in accordance with Koop's phenomenological theory [16-18]. It is well known that ferrites are composed of well-defined grains and separated by grain boundaries. The grains are known to be conducting while the grain boundaries are highly resistive. The main mode of conduction in ferrites is the electron hopping between ions of the same element present in more than one valency state at crystallographic equivalent lattice sites and this is commonly termed as Verwey mechanism of electron hopping [19].

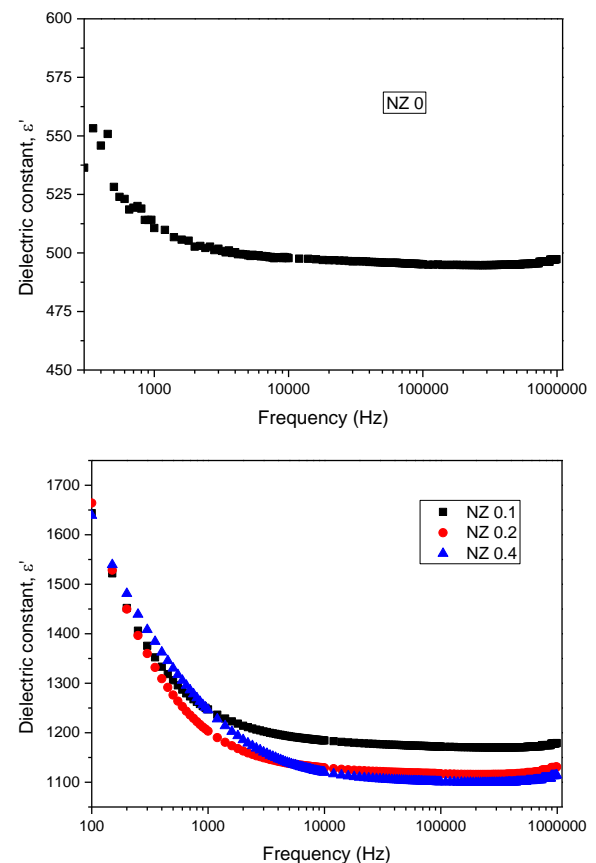


**Fig. 4.** Variation of dielectric constant with frequency

In the present case, hopping of electrons take place between  $Fe^{2+}$  and  $Fe^{3+}$  ions at the B-sites since  $Fe^{2+}$  ions formed at the time of sintering are present only at the B-sites. The high resistive or non-conductive

grain boundaries block the mobile charge carriers and inhibit charge migration leading to piling up of charges at the grain boundary thereby causing polarization [16-18, 20]. At low frequencies of an applied field, a net oscillation of charges between barriers producing a very large capacitance and hence a large dielectric constant [20], as has been observed. As the frequency of the applied field increases, the electrons reverse their direction of motion more often which decreases the probability of electrons reaching the grain boundary and as a result the polarization decreases [21]. Hence, the observed decrease in the dielectric constant (shown in Fig. 4). At much higher frequencies of the applied field, the electronic hopping could not follow the frequencies of the alternating field, and therefore a low and nearly constant value of the dielectric constant is expected [22], and has been obtained.

The variation of dielectric loss ( $\tan\delta$ ) as a function of frequency in the range 100Hz -1MHz is depicted in Fig. 5. It can be seen that the loss tangent decrease continuously with increasing frequency. None of the samples exhibit loss peak. The decrease of  $\tan\delta$  with frequency can be explained in accordance with Koop's phenomenological model [17] as discussed above. As the frequency of the applied electric field increases, the hopping frequency of the charge carrier cannot follow the alternating field and become independent of it and as a result the value of  $\tan\delta$  decreases [23, 24].

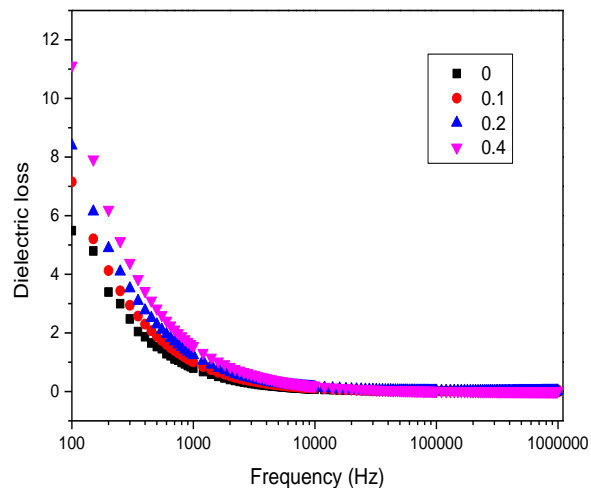


Fig. 5. Variation of dielectric loss with frequency.

### DC resistivity measurement

The variation of room temperature DC resistivity with  $\text{Zn}^{2+}$  substitution is shown in Fig. 6. It is observed that the value of DC resistivity decreases with the increase of  $\text{Zn}^{2+}$  content. Resistivity in ferrites is explained by the electron hopping mechanism between  $\text{Fe}^{2+}$  and  $\text{Fe}^{3+}$  ions at B-site. The decrease in resistivity may be understood in terms of the substitution of  $\text{Zn}^{2+}$  ions and the cation distribution.  $\text{Zn}^{2+}$  prefer to occupy the tetrahedral A site,  $\text{Ni}^{2+}$  the octahedral B site, while  $\text{Fe}^{3+}$  ions

partially occupy A and B sites. The cation distribution may be assumed as  $(\text{Zn}_x\text{Fe}_{1-x})[\text{Ni}_{1-x}\text{Fe}_{2+x}]$  [24]. On increasing  $\text{Zn}^{2+}$  concentration at A sites,  $\text{Ni}^{2+}$  concentration at B sites will decrease. This leads to migration of some  $\text{Fe}^{3+}$  ions from A site to B site to balance the reduction in  $\text{Ni}^{2+}$  ions concentration at B sites. The  $\text{Fe}^{2+}$  ions that may have been formed has B-site preference. As a result, the number of  $\text{Fe}^{3+}$  and  $\text{Fe}^{2+}$  ions at B sites which are responsible for electrical conductivity in ferrites increase and consequently resistivity decreases [25-27].

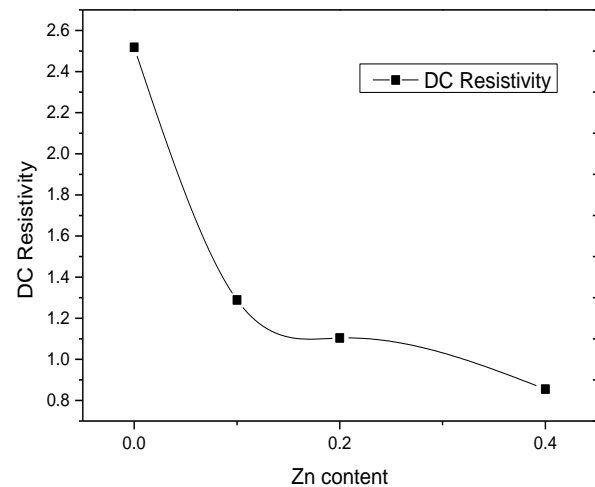


Fig. 6. Variation of DC resistivity with Zn content.

### Conclusion

A series of Zn substituted Ni-ferrites were successfully synthesized by chemical sol-gel method. X-ray diffraction confirmed the formation of single phase spinel structure of all the samples. Lattice parameter and crystallite size were calculated from the XRD data. The dielectric constant and loss decrease with the increase of frequency and attains constant value as the frequency increases. The value of DC resistivity decreases with the increase of Zn substitution.

### Acknowledgements

The authors would like to acknowledge the XRD and SEM Central Facilities of Manipur University.

### References

1. Smit, J.; Wijn, H. P. J.; *Philips Tech. Lib.*, **1959**, 136.
2. Gorter, E. W.; *Adv. Phys.*, **1957**, 6, 336.
3. Mamta, M.; Ph D Thesis, Manipur University **2006**.
4. Dixit, G.; Singh, J. P.; Srivastava, R. C.; Agrawal, H. M.; Chaudhary, R. J.; *Adv. Mat. Lett.*, **2012**, 3, 21.
5. Goldman, A. (Eds.); *Modern Ferrite Technology*; Springer Science and Business Media: USA, **2006**.
6. Jun, X.; Xiang-Qian, S.; Fu-Zhan, S.; Ming-Quan, L.; *Chinese Physics B*, **2009**, 18, 4960.
7. Verma, A.; Goel, T. C.; Mendiratta, R. G.; Gupta, R. G.; *J. Magn. Mater.* **1999**, 192, 271.
8. Kumar, A.; Kumar, P.; Rana, G.; Yadav, M. S.; Pant, R. P.; *Appl. Sci. Lett.* **2015**, 2, 33.
9. Deka, S.; Joy, P. A.; *Mater. Chem. Phys.*, **2006**, 100, 98.
10. Kurian, M.; Thankachan, S.; Nair, D. S.; Aswathy, E. K.; Babu, A.; Thomas, A.; KT, B. K.; *J. Saudi Chem. Soc.*, **2013**, 4, 199.

11. Ahmmed, M. A.; Afify, H. H.; Zawawai, I. K. El.; Azab, A. A.; *Magn. Magn. Mater J.*, **2012**, 324, 2199.
12. Reddy, P. V. B.; Ramesh, B.; Reddy, Ch. G.; *Physica B*; **2010**, 405, 1852.
13. Gorter, E. W.; *Philips Res. Rep.*, **9**, 1954, 9, 308.
14. Yadoji, P.; Peelamedu, R.; Agrawal, D.; Roy, R.; *Mater. Sci. Engg. B*, **2003**, 98, 269.
15. Maxwell, J. C. (Eds.); *Electricity and Magnetism*; Oxford University Press: UK, 1881.
16. Wagner, K. W.; *Ann. Phys. (Laipzig)*, **1993**, 40, 817.
17. Kooops, C. G.; *Phys. Rev.*, **1951**, 83, 121.
18. Verwey, E. J. W.; Haayman, P.W.; Romeijn, F. C.; *J. Chem. Phys.*, **1947**, 15, 181.
19. Hench, L. L.; West, J. K. (Eds.); *Principles of Electronic Ceramics*; John Wiley & Sons: USA, **1990**.
20. Singh, A. K.; Goel, T.C.; Mendiratta, R. G.; Thakur, O. P.; Prakash, C.; *J. Appl. Phys.*, **2002**, 91, 6626.
21. Rao, B. P.; Rao, K. H.; Trinadh, K.; Caltun, O. F.; *J. Optoelec and Adv. Mater.*, **2004**, 3, 951.
22. Rezlescu, N.; Prakash, C.; Prasad, G.; *J. Phys. D: Appl. Phys.*, **2006**, 39, 1635.
23. Verwey, E. J. W.; de Boer, J. M.; *Rec. trav. Chim-Pays-Bas*, **1936**, 55, 531.
24. Blaise, G.; *Phillips Res. Rep.*, **3**, 1964.
25. Gorter, E. W.; *Philips Res. Rep.*, **9**, 1954.
26. Islam, M. U.; Abbas, T.; Niazi, S. B.; Ahmed, Z.; Sabeen, S.; Chaudhry, M. A.; *Solid State Commun.*, **2004**, 130, 353.
27. Joshi, G.; Khot, A.; Sawant, S.; *Solid State Commun.*, **1998**, 65, 1593.